Applied Energy 362 (2024) 122953

Contents lists available at ScienceDirect

Applied Energy

journal homepage: www.elsevier.com/locate/apenergy

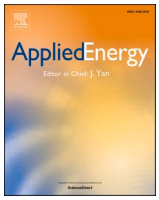

Experimental investigation of low-temperature fluidised bed thermochemical energy storage with salt-mesoporous silica composite materials

Xiao Liu [a], Xin Liu [a,b,*], Fangming Yang [a], Yupeng Wu [a,*]

[a] Faculty of Engineering, University of Nottingham, Nottingham NG7 2RD, United Kingdom
[b] School of Engineering, University of Lincoln, Brayford Pool, Lincoln LN6 7TS, United Kingdom

HIGHLIGHTS

- A salt-composite-based fluidised bed system was developed for low temperature TCES.
- CMS-based salt composites exhibited good fluidisability with a low u_{mf} of around 0.01 m/s.
- $CaCl_2$/CMS composite attained a high ESD of 1508 kJ/kg when hydrated under 30 °C and 60% RH.
- $CaCl_2$/CMS composites demonstrated good cyclic stability in the fluidised bed system.

ARTICLE INFO

Keywords:
Fluidised bed
Fluidisation
Composite 'salt in porous matrix' (CSPM)
Commercial mesoporous silica (CMS)
Thermochemical energy storage (TCES)
Energy storage density (ESD)

ABSTRACT

Low-temperature thermochemical energy storage (TCES) with composites 'salt in porous matrix' (CSPMs) is widely recognized as a sustainable and efficient solution for harnessing low-grade heat and off-peak electricity. However, many high-performance CSPMs described in the literature have been produced in powder form with particle sizes below 50 μm, which makes them unsuitable for direct use in conventional fixed-bed or fluidised-bed systems. Fluidised-bed systems, highly regarded for their rapid heat and mass transfer advantages, have been extensively used in high-temperature TCES. However, their potential for low-temperature TCES applications remains unexplored due to the lack of suitable thermochemical sorption materials. In this work, we aim to investigate the feasibility of fluidised-bed TCES systems for low-temperature TCES applications using the self-developed fluidisable and high-performance CSPMs. A series of CSPMs were prepared using a commercial mesoporous silica (CMS) as the host matrix and $CaCl_2$, $MgSO_4$ and $MgBr_2$ as the salts, with the same salt loading level of 50 wt% and particle size range of 150–300 μm. A lab-scale fluidised-bed TCES system was constructed for a comprehensive assessment of the material properties, including minimum fluidisation velocity (u_{mf}), water adsorption capacity, temperature lift, and energy storage density (ESD). The results show that the salt/CMS composite powders can be easily fluidised with a u_{mf} of approximately 0.01 m/s and provide efficient solid mixing during bubbling fluidisation. Among the tested CSPMs, the $CaCl_2$/CMS composite shows the best heat-discharging performance. Specifically, the $CaCl_2$/CMS composite, when hydrated at 30 °C and 60% relative humidity, has a ESD of 1508 kJ/kg (equivalent to 264 kWh/m^3) and provides a maximum bed temperature of 58 °C. In addition, it exhibits excellent stability for use in the fluidised-bed system, with similar fluidisation characteristics and ESDs after multiple cycles of heat charging and discharging processes. This work is believed to inspire future research on the development of CSPM powders.

1. Introduction

In the United Kingdom, nearly a quarter (23%) of the total greenhouse gas emissions originate from the heating of buildings, and a vast majority (88%) of households currently rely on natural gas for heating [1]. Thermochemical energy storage (TCES) systems are considered as one of the key technologies for decarbonising the building sector and increasing the share of renewable energy sources. In practice, TCES systems can be used in combination with solar thermal collectors [2],

* Corresponding authors at: Faculty of Engineering, University of Nottingham, Nottingham NG7 2RD, United Kingdom.
E-mail addresses: xliu@lincoln.ac.uk (X. Liu), yupeng.wu@nottingham.ac.uk (Y. Wu).

https://doi.org/10.1016/j.apenergy.2024.122953
Received 23 December 2023; Received in revised form 23 February 2024; Accepted 1 March 2024
Available online 15 March 2024
0306-2619/© 2024 The Authors. Published by Elsevier Ltd. This is an open access article under the CC BY license (http://creativecommons.org/licenses/by/4.0/).

Nomenclature

CMS	Commercial mesoporous silica
CSPM	Composites 'salt in porous matrix'
ESD	Energy storage density
DSC	Differential scanning calorimeter
FB-TCES	Fluidised bed thermochemical energy storage
PCM	Phase change material
RH	Relative humidity
TGA	Thermogravimetric analysis
TCES	Thermochemical energy storage
ESD_g	Gravitational energy storage density, kJ/kg
ESD_v	Volumetric energy storage density, kWh/m^3
Q_{dis}	Useful sorption heat during discharge process, kJ
C_p	Specific heat capacity, kJ/kg K
q_m	Mass flow rate, kg/s
ρ_b	Bulk density, kg/m^3
m	Sample' weight, kg
r	Mixing ratio, kg/kg
$e(T)$	Actual partial vapour pressure, hPa
$e_s(T)$	Saturation vapour pressure, hpa
p	Total air pressure, hPa
T	Temperature, °C
S_{BET}	Specific surface area, m^2/g
V_{total}	Total pore volume, cm^3/g
$\Delta T_{bed,\ max}$	Maximum bed temperature lift, °C
$\Delta T_{air,\ max}$	Maximum air temperature lift, °C

grid-photovoltaic hybrid systems [3], thermoelectric generators [4], air conditioning units [5–7] or building facades [8] to store renewable energy, recover waste heat, and provide heating, cooling and/or electricity generation. This integration helps store excess thermal energy during off-peak periods and reduce energy costs during high-demand periods. In comparison to the traditional approaches that use water or phase change material (PCM) as the heat storage medium, TCES systems can be designed to be more compact in size, due to the high energy density of thermochemical materials (i.e., >1 GJ/m^3 theoretically and 5–20 times higher than that of sensible/latent heat storage materials) [9,10]. Also, TCES systems offer the benefit of negligible heat losses during long-term storage, as the heat is preserved as chemical potential [11].

TCES consists of three steps: heat charging, storage and discharging, which are implemented through a reversible chemical reaction or desorption/sorption process ($AB + heat \leftrightarrows A + B$) [12]. Solid (sorbent)-water vapour (sorbate) is the most prevalent working pair for sorption-type TCES towards low-temperature applications (30–150 °C) [11,13]. The solid sorbents reported in literature can be classified into three groups: physisorption, chemisorption and composite materials.

Physisorption is the process whereby water molecules are adhered to the adsorbent surface with weak binding forces (e.g., Van der Waals forces), which can be reversed by applying heat or vacuum [14]. Since physisorption is a surface process, the water adsorption capacity is governed by the material's structure and surface properties such as porosity and specific surface area [15–17]. Zeolites are a class of crystalline aluminosilicate microporous materials with over 250 framework types according to the International Zeolite Association (IZA) [18], among which zeolite X-type with a relatively low silica/aluminium (Si/Al) ratio and strong hydrophilic character is the most used for low-temperature heat storage purposes [13,19,20]. Mette et al. [21] set up a lab-scale TCES system with zeolite 13X beads and observed a surge in the reactor bed temperature from 30 to 108 °C at an inlet water vapour pressure of 30 mbar. Padamurthy et al. [22] compared the performance of a TCES system with two different zeolites and revealed that the pellets of zeolite 13X performed better than zeolite 4A in terms of energy density (45.2 vs. 17.8 kWh/m^3) and energy efficiency (44.1% vs. 24.0%). Mahon et al. [23] measured the energy densities of zeolite 13X received as fine powder (with 3–5 μm diameters) and pellet (with a 3.2 mm diameter) to be 589 and 479 J/g, respectively, by using a differential scanning calorimeter (DSC) with a temperature ramp from 20 to 150 °C. In line with the previous study [23], Touloumet et al. [19] obtained higher energy density and water sorption capacity for binder-free zeolite 13X powder (1080 J/g and 0.31 g/g), compared to zeolite 13X beads containing 20% binder (1007 J/g and 0.28 g/g) and fine powder crushed from the beads (980 kJ/kg and 0.28 g/g), over a DSC temperature ramp range of 20–300 °C. Moreover, the binder-free zeolite 13X powder exhibited the fastest water uptake, followed by the crushed powder, then the beads [19]. The researchers elucidated that adding binder to zeolite 13X altered its textural properties, such as average pore size, volume of micropores and surface area. These changes can affect the physisorption capacity and rate. A reactor-scale experiment by Bardy et al. [24] demonstrated that zeolite 13X with binders, in the forms of pellet and crushed powder, had comparable water sorption capacities but different sorption rates and heat discharging performance.

Chemisorption is another kind of surface adsorption in which strong chemical bonds (e.g., valency forces) form between sorbent and sorbate, usually with more heat released (or larger enthalpy) than physisorption [10]. Salt hydrates are a category of chemisorption materials. Their working mechanism can be expressed as $Salt \cdot (m+n)H_2O_{(s)} + heat \leftrightarrows Salt \cdot mH_2O_{(s)} + nH_2O_{(g)}$, where a salt hydrate undergoes water desorption upon heating and is converted into its less hydrous or anhydrous state [9,13]. Physisorption materials such as zeolite 13X and silica gel have limited energy densities, normally not exceeding 900 J/g when using low-temperature heat sources for water desorption (≤150 °C) [25]. Magnesium sulphate heptahydrate ($MgSO_4{\cdot}7H_2O$) and hexahydrate ($MgSO_4{\cdot}6H_2O$) are known for their high theoretical energy densities (2.2–2.8 GJ/m^3) and can be easily dehydrated to lower hydrates, for example, to $MgSO_4{\cdot}0.3H_2O$ at 150 °C [26–28]. However, $MgSO_4$ has slow hydration kinetics and poor heat discharging performance (i.e., the maximum temperature lifts are 4–10 °C) [27,29]. Calcium chloride hydrates ($CaCl_2{\cdot}nH_2O$, n = 0, 2, 4, 6) are another promising salt hydrates with high theoretical energy densities (1–3 GJ/m^3 [30]). In contrast to $MgSO_4$, the hydration process of $CaCl_2$ is fast and the higher hydrates can form at low vapour partial pressures, which makes it possible to fully recover the stored thermal energy and attain high energy efficiency. Nevertheless, similarly to other chloride-based salts like magnesium chloride ($MgCl_2$) and strontium chloride ($SrCl_2$), $CaCl_2$ is deliquescent, and in other words, the higher hydrates tend to become liquid, which gives rise to a series of problems such as salt agglomeration, reduction of permeability, deterioration of material performance, and corrosion.

To achieve high energy density while avoiding the negative impacts of salt deliquescence, an effective and facile method is to develop composites 'salt in porous matrix' (CSPMs). Successful development of CSPMs imposes high requirements on the selected porous materials, for example, they should have the capability to take on a high salt concentration with no or minimal blockage of pores and leakage of salt solution; they should also have appropriate particle sizes and good thermophysical properties (e.g., high thermal conductivity and permeability) to suit specific reactor designs and ensure efficient heat and mass transfer in reactors. Various porous materials have been proposed as host matrices for salt impregnation, however, some of which do not meet the above-mentioned requirements, and some of which show enormous potential at the material level but have not been adequately evaluated

on a reactor scale.

Traditional CSPMs such as zeolites with $MgSO_4$ are typically prepared with low salt contents (5–15 wt%) because excess salt can clog the micropores and hinder water diffusion in the zeolite structure, resulting in lower water uptake [26,31,32]. At low humidity levels, zeolites with hygroscopic salts such as $CaCl_2$ and $MgCl_2$ behave similarly to zeolites with $MgSO_4$. However, at medium or high humidity levels, the water uptake initially decreases and then increases with a higher salt concentration [33,34]. This is because deliquescence occurs and a higher salt load enables the formation of a significant amount of saturated salt solution in pores, and consequently, the absorption of wate vapour into the solution overcompensates the pore blockage effect [33,34]. Nonnen et al. [34] confirmed this phenomenon through a reactor experiment using a packed bed of zeolite beads impregnated with 15 wt% $CaCl_2$. Despite the increase in water uptake and energy density at higher humidity, the authors noticed that some of the aqueous $CaCl_2$ solution leaked from the beads when the vapour partial pressure reached 33 mbar (equivalent to the relative humidity of 78% at 30 °C). Traditional silica gels with small pore diameters (<2–3 nm) have the same limitations [35,36]. Accordingly, it is not recommended to use microporous materials for preparing CSPMs. Macroporous materials such as vermiculite and expanded graphite can hold large amounts of salt (68–87%) because of their large pore sizes (>50 nm) [37]. On the other hand, they are susceptible to liquid leakage and particle aggregation, because the formed salt solution can easily leak from the large pores and adhere to the external surface of particles [37].

In recent years, several studies have been conducted to fabricate CSPMs using mesoporous materials (with 2–50 nm pore diameters) for enhanced performance and stabilisation. Successful examples include mesoporous silica [38], mesostructured cellular foam (MCF) [32], and metal-organic frameworks (MOFs) such as MIL-101(Cr) [39] and aluminium fumarate [40]. Nevertheless, many of the CSPMs are available as fine powders with small particle sizes ranging from 0.1 to 100 μm and have only been evaluated at the material level. To the authors' best knowledge, there is no research demonstrating the performance of 'salt in mesoporous matrix' composites as fine powders when incorporated into TCES systems and tested under different operating conditions.

The key to successfully implementing TCES systems lies in finding the right combination of thermochemical material, particle technology, and system operating conditions (e.g., working air temperature, humidity and flow rate) to achieve optimal performance. Traditional TCES systems usually use packed-bed configurations, with coarse particles stacked in a stainless-steel cylinder to exchange heat and moisture with hot, dry (or cool, humid) airflow. Fluidised beds are an important solid-gas contacting technology employed in various industrial applications such as combustion, desiccation and solar thermal energy storage [41]. In comparison to packed-bed reactors, fluidised-bed reactors offer several advantages. These include enhancing heat and mass transfer between solid and gas, and addressing issues such as uneven reaction, overhydration and hot spots [12,42–45]. Fluidised-bed reactors have been widely utilised in concentrated solar power (CSP) plants, usually combined with chemical-reaction-based TCES systems such as calcium hydroxide/calcium oxide ($Ca(OH)_2/CaO$) systems operating at high temperature levels (400–1000 °C) [46]. There are few studies utilising zeolite 13X [24] and zeolite/$MgCl_2$ composite [47] in fluidised beds for low-temperature TCES applications. However, the zeolite-based TCES systems require heat charging temperatures between 180 and 300 °C to achieve a satisfactory ESD of up to 900 kJ/kg and thermal efficiency of up to 80% [25]. This limits their widespread use in buildings, as they cannot efficiently be charged with low-grade thermal energy such as solar energy (i.e., flat-plate and evacuated-tube solar collectors in buildings typically operate within the range of 80 to 200 °C [48]). In contrast, the CSPMs, consisting of mesoporous materials impregnated with salts such as $MgSO_4$ and $CaCl_2$, can be almost completely dehydrated and regenerated at temperatures below 200 °C [32,40,49]. Li et al. [50] introduced a cascaded solar thermal energy storage with multiple salt sorbents ($CaCl_2$, $SrCl_2$, $SrBr_2$ and $MnCl_2$), which can achieve an energy density of over 1200 kJ/kg when using an external heat source temperature of 161 °C.

While there is a lot of literature on mesoporous-matrix-based CSPMs, many of them are in powder form with particle sizes below 50 μm, belong to Geldart Group C and exhibiting poor fluidisability due to strong inter-particle cohesion. This presents a challenge when attempting to use them in either packed-bed or conventional fluidised-bed TCES systems. On the other hand, fine and ultrafine powders have large surface-to-volume ratios, enabling better contact efficiency and higher reaction rates per unit volume of reactor compared to coarse particles [51,52]. The fluidisation of Geldart Group C particles can be made possible or improved by the assistance of external forces/fields such as vibration, stirring, and acoustic/electric/centrifugal fields [51–53]. For example, Raganati et al. [54,55] used acoustic fields with different sound intensities (120–150 dB) and frequencies (50–300 Hz) to promote the break-up of the large aggregates yielded by cohesive forces and to improve the fluidisation of fine powders. The sound-assisted fluidisation technique is highly economical and only requires extra equipment (e.g., signal generator, audio amplifier, loudspeaker and oscilloscope) easily available on the market [54]. However, it may not be suitable for use in buildings that require a noise-less environment. Mixing Geldart Group C particles with a small portion of inert easy-to-fluidise particles (Geldart Group A or B) is another method to achieve smooth fluidisation [46], but it has limitations, especially for processes where contamination should be avoided [53].

The challenge with using fluidised bed systems for low-temperature TCES is to find an appropriate storage material that encompasses the features of large energy density, high temperature lift, good fluidisability and good stability, and is commercially available. In our previous study, a series of novel CSPMs were developed based on a commercial mesoporous silica (CMS) with particle sizes ranging between 150 and 300 μm [49]. The thermogravimetric analysis (TGA) experiments revealed that the CSPMs with a high salt loading level of 50 wt% have both high water sorption capacities and rates, indicating great potential for TCES. Following our previous work, this study will, for the first time, evaluate the system-level performance of the developed CSPMs, with a focus on fluidisation behaviours and thermal characteristics. For this purpose, three CSPMs consisting of CMS impregnated with $CaCl_2$, $MgSO_4$ and $MgBr_2$ were prepared and evaluated using a self-developed fluidised-bed-based TCES system. The evaluation criteria include fluidisation quality, water sorption capacity and kinetics, temperature lift, ESD and cyclic stability. The material performance has also been assessed under various system operating conditions, including different dehydration/hydration temperatures, relative humidities, and flow rates.

2. Materials and methods

Prior to the experiments, a material screening process was undertaken to select appropriate materials for the formulation of 'salt in porous matrix' composites guided by specific criteria. The chosen salt is required to be cost-effective, safe, and easily manageable. Moreover, it needs to exhibit high ESD, rapid hydration/dehydration kinetics, and compatibility with a designated working temperature. The porous matrix needs to be commercially available and amenable to fluidisation.

Table 1 summarizes the thermal-physical properties and performance of some CSPMs developed in previous studies. Notably, the cost-effective salts such as $MgSO_4$ and $CaCl_2$, characterized by high ESDs and stability with dehydration temperatures below 200 °C, have been widely used to prepare salt composites for TCES. The CSPMs consisting of strontium-based salts such as $SrBr_2$ demonstrate high reaction enthalpies, but their high prices might be a major barrier for large-scale applications. Our previous study has identified $MgBr_2$ as a viable candidate salt for salt composite formulation, owing to its fast reaction kinetics and high water sorption capacity. Accordingly, $CaCl_2$, $MgSO_4$

Table 1
Specifications of the thermochemical sorption materials reported in literature.

Material		Particle information	Pore properties			TGA/DSC measurement		Experimental setup	Lab-scale reactor experiment		Ref
Category / Type	Salt content (wt%)	Size (mm)	Average pore size (nm)	Total pore volume (cm^3/g)	Surface area (m^2/g)	Water uptake (g/g)	Heat of dehydration / hydration (J/g)		ΔT_{max} (°C)	ESD_v (kWh/m^3) / ESD_g (kJ/kg)	
$MgSO_4$ + Zeolite 13X	15	2	–	–	–	0.15	-	Fixed bed	26	166 (0.18 Wh/g)	[26]
$MgSO_4$ + Zeolite Na-X	15	1.6–2.5	–	0.08	204	–	731 / -	TG-DSC	–	–	[31]
$MgSO_4$ + MCF	50	–	29	0.25	140	0.50	–	TGA	–	–	[32]
$SrBr_2$ + EVM	63	5–20	–	–	–	0.53	1656 (0.46 Wh/g) / -	Humidity chamber	–	–	[56]
$SrBr_2$ + EG-TSA	90	–	–	–	–	0.44	–	TGA	–	189 / 864 (0.24 Wh/g)	[57]
$SrBr_2$ + MIL-101(Cr)	63	–	–	0.44	603	0.30	- / 1350 (0.375 Wh/g)	IGA	–	–	[58]
$SrCl_2$ + SG	10	3	1.0	0.36	581	0.34	–	Fixed bed (plate reactor)	19	97 / 299	[36]
$MgCl_2$ + Zeolite Na-X	15	1.6–2.5	–	0.16	349	–	921 / -	TG–DSC	–	–	[16]
$MgCl_2$ + $CaCl_2$ + zeolite 13X	15 (1:1.5)	3–5	–	–	–	–	–	Fixed bed	46	- / 719	[59]
$CaCl_2$ + WSS	22	–	4–20	0.15	38.4	1.10	–	Mesoporous ceramic honeycomb filter	26	328 (1181 MJ/m^3) / 2549	[60]
$CaCl_2$ + EG	48	8 μm	219	0.63	11.5	0.79	1638 / -	Thermostat cabinet	–	–	[61]
$CaCl_2$ + MIL-101 (Cr)	47	–	–	0.34	242	0.47	1118 / -	Constant temperature and humidity system	–	–	[39]
$CaCl_2$ + AF	58	0.1–0.5 μm	–	0.18	107	0.68	1840 / -	TG-DSC	–	–	[40]
$CaCl_2$ + SG	43	0.1–0.25	20	0.38	75	0.40	- / 1080 (0.3 Wh/g)	IGA	–	–	[38]
$CaCl_2$ + CMS	50	0.15–0.3	21.8	0.40	78	1.08	–	TGA	–	–	[49]
$MgSO_4$ + CMS	50	0.15–0.3	23.4	0.46	88	0.47	–		–	–	
$MgBr_2$ + CMS	50	0.15–0.3	18.8	0.59	122	0.37	–		–	–	

MCF: mesostructured cellular foam.
EVM: expanded vermiculite.
EG: expanded graphite.
EG-TSA: expanded natural graphite treated with sulfuric acid.
WSS: wakkanai siliceous shale.
AF: aluminium fumarate.

and $MgBr_2$ were selected for preparing CSPMs in this study. With respect to the porous matrices, as shown in Table 1, most porous materials have particle diameters that are either too small (<10 μm) or excessively large (>1 mm) to facilitate optimal fluidisation, except for the CMS (150–300 μm). In addition, the CMS has a sufficiently large pore size, pore volume and surface area, allowing for large salt impregnation (up to 50 wt% [49]).

In this study, three composite materials consisting of the CMS impregnated with $CaCl_2$, $MgSO_4$ and $MgBr_2$ were developed for fluidisation and hydration tests. For comparison, zeolite 13X and $CaCl_2$/zeolite composite with similar particle sizes as the CMS-based composites were prepared and chosen as the reference materials.

2.1. Preparation of salt composites

CMS based salt composites: commercial mesoporous silica (CMS) with particle diameters in the range of 150–300 μm was purchased from PQ Silicas UK Ltd. Anhydrous $CaCl_2$ was purchased from Fisher Scientific UK Ltd. The proposed $CaCl_2$/CMS composites with a high salt loading level of 50 wt% was prepared via an incipient wetness impregnation method [32,49]. Prior to impregnation, CMS was first dried at 100 °C for overnight to remove residue moisture. In a typical procedure, 25 g of anhydrous $CaCl_2$ was first dissolved in 200 mL DI water and then 25 g of dried CMS was mixed with the $CaCl_2$ solution. The mixture was left at room temperature under continuous stirring until all the water was evaporated. The white powder was then dried in a vacuum oven at 150 °C for 6 h to allow the complete dehydration of $CaCl_2$. The dehydrated powder (see Fig. 1a) was collected and stored in a sealed bottle before testing. Similar methods were used to prepare the other two composites: $MgSO_4$/CMS and $MgBr_2$/CMS with a same salt loading level of 50 wt%.

Zeolite 13X based salt composites: in this work, zeolite 13X was also

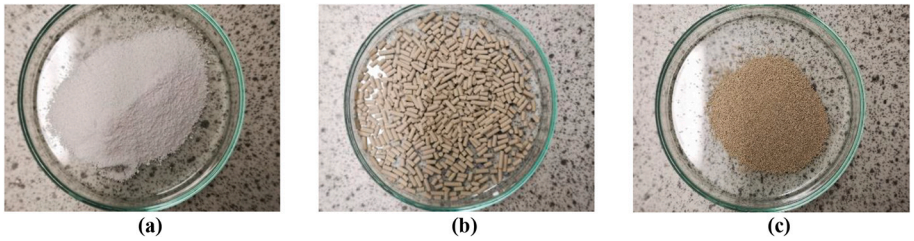

Fig. 1. Photos of (a) the $CaCl_2$/CMS composite powder in dry state, (b) the zeolite 13X pellets, and (b) the zeolite 13X powder crushed from the pellets.

used as a porous matrix to prepare a salt composite. Zeolite 13X pellets with a mean diameter of 1.6 mm (see Fig. 1b) purchased from Sigma-Aldrich were first ground and sieved to obtain zeolite 13X powder with particle sizes between 212 and 425 μm (see Fig. 1c). The crushed powder was dried in a vacuum oven at 150 °C for 6 h to remove the sorbed moisture and then stored in a sealed bottle. Given the much smaller pore volume and pore size than CMS, $CaCl_2$/zeolite salt composite with a maximum salt loading level of 15 wt% was prepared by using the same incipient wetness impregnation method.

2.2. Lab-scale fluidised bed TCES system for material evaluation

2.2.1. Experimental set up

Fig. 2 shows the schematic diagram of a lab-scale fluidised-bed based TCES system for material evaluation. The system mainly comprised of a fluidised bed reactor, a compressed air supply system (not displayed in the figure), an air humidification section, an environmental temperature control chamber, and sensors. The fluidised bed reactor consisted of a 300-mm-high, 40-mm-diameter cylinder and two conical sections, the flanges of which were jointed together with a silicone rubber gasket placed in-between to ensure a tight seal. The cylinder was 3D printed using a transparent ABS (acrylonitrile butadiene styrene) filament to fulfil the needs for visual observation and high resistance to heat and chemicals, while the other reactor components like the flanges were 3D printed using an ASA (acrylonitrile styrene acrylate) filament for higher durability. Two borosilicate glass filter discs with a porosity grade of 2 were installed at the bottom and top of the cylinder to prevent particles from escaping. The cylinder was covered with a 26 mm thick layer of nitrile rubber insulation with a thermal conductivity of 0.034 W/m·K to reduce heat losses. Two PT100 probes were installed in the reactor: one was immersed in the solid bed (at 30 mm height from the cylinder bottom) to measure the bed temperature, and the other was positioned above the solid bed (at 110 mm height from the cylinder bottom) to measure the air temperature.

The designed TCES system is an open system where the gas reactant is taken from and released to the ambient. Dry compressed air with RHs of 2–3% at 25 °C was introduced into the system. The air flow rate was maintained at 6 L/min using a GFC37 mass flow controller. The air temperature increased to approximately 30 °C, as it flowed through a long stainless-steel pipe (1 → 2 → 4) in a controlled environmental chamber set at 30 °C. In hydration tests, a three-way T-port ball valve was used to split the airflow into two streams. One stream followed the

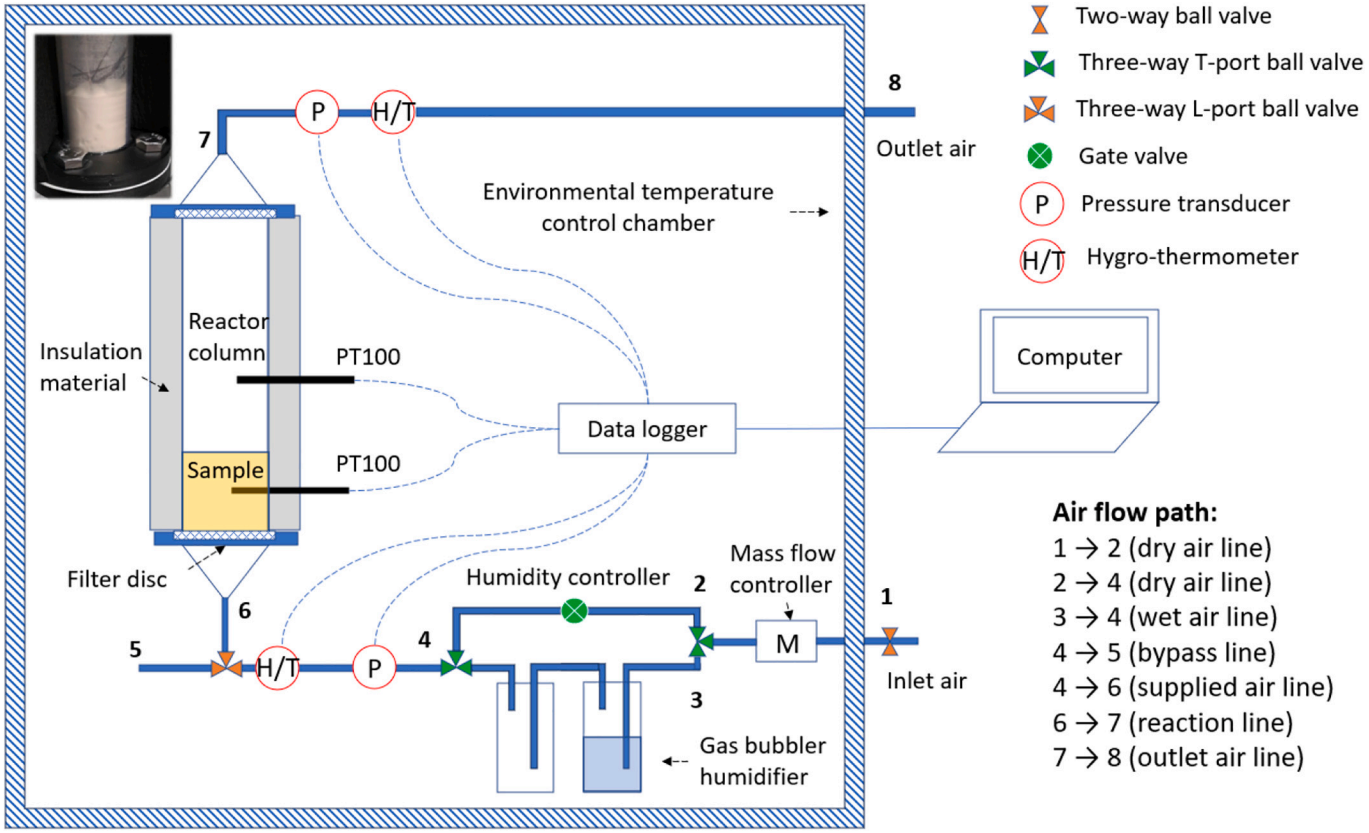

Fig. 2. Schematic diagram of the experimental setup for fluidisation and hydration (/heat discharging) tests.

original dry pathway (1 → 2 → 4), and the other was bubbled through a vessel containing water (1 → 3 → 4). A water trap was placed behind the gas bubbler humidifier to prevent liquid water from entering the downstream pipelines. The two streams mixed at the second three-way T-port ball valve (point 4), and the mixing proportion was determined by the opening percentage of the gate valve located in the dry pathway. For example, when the gate valve was fully closed, all the inlet air was directed to the wet pathway (i.e., 100% wet air), and the air humidity (at point 4) reached a maximum value (e.g., approximately 98% measured at 30 °C). Behind the air humidification section, a pressure transducer measured the gauge pressure of the mixed air, and a hygro-thermometer measured the air temperature and relative humidity. The bypass line (4 → 5) allowed for the desired hydration conditions to achieve and stabilise. After stabilisation, the airflow was directed to the reaction line (4 → 6) using a two-way L-port ball valve. The humidity and temperature of the released air were recorded using a hygro-thermometer in the outlet air line (7 → 8). All the sensors were connected to a data logger for data acquisition at 10 s time intervals. The specifications of the sensors are described in Table 2.

2.2.2. Experimental procedures

To characterise the developed sorption materials, the following experiments and analysis have been conducted:

- **Procedures of the fluidisation experiment**: (1) a 30 g dry sample was placed in the reactor; (2) dry air was supplied to the reactor, and its flow rate was gradually increased from 1 to 10 L/min with increments of 1 L/min; (3) the gauge pressures of the inlet and outlet air at each flow rate was measured; (4) the pressure drop of the airflow through the sample-filled reactor and sensors was calculated; (5) the pressure drop was also recorded for the test with an empty reactor at each flow rate, (6) the pressure drop across the solid bed in the reactor can be calculated by taking the difference between the results from steps 4 and 5.
- **Procedures of the hydration experiment**: (1) a 30 g sample that had been dehydrated at 150 °C for 6 h was placed in the reactor; (2) humid air was delivered to the reactor at a constant flow rate of 6 L/min, hydration temperature of 30 °C and RH of 60%; (3) the temperatures of the solid bed and airflow in the reactor (detected by the PT100 sensors shown in Fig. 2) as well as the RH and temperature of the outlet air (detected by the hygro-thermometer) were recorded; (4) the experiment was terminated when the air temperature lift dropped to below 2 °C or the experiment period exceeded 10 h; (5) the ESD of the sample, as well as the ratio of the moisture concentration in the outlet air to that in the inlet air (*CR*), were calculated using the below equations.
- **Parametric analysis**: a series of hydration tests were conducted under different conditions: (1) RHs — 20%, 40% and 60%, (2) hydration temperatures — 18, 24 and 30 °C, (3) air flow rates — 2, 6 and 10 L/min, (4) dehydration temperatures — 80, 100, 120 and 150 °C.

Table 2
Specification of the measurement devices.

	Model	Supplier	Range	Accuracy
Hygro-thermometer	HC2A-IE02	Rotronic Instruments Ltd.	−100–200 °C 0–100% rh	± 0.8% rh/ ± 0.1 °C
Mass flow controller	GFC37	Aalborg Instruments & Controls, Inc.	0–30 L/min	± 1% of full scale
PT100 sensor	Customised	Alphatemp technology Ltd.	−75–250 °C	± 0.15 °C
Gauge pressure transducer	dTRANS p30	Jumo UK Ltd.	0–0.25 bar	± 0.5% max. of full scale
Data logger	DT85 series 4	Omni Instruments Ltd.	–	–

- **Other measurements**: (1) the temperature distribution of the fluidised bed was evaluated using a FLIR E6 thermal imaging camera; (2) the material stability was investigated by running 5 consecutive cycle tests of hydration (at 60%, 30 °C, 6 L/min) and dehydration (at 150 °C).

The thermal energy released by the solid bed and transferred to the airflow can be determined by Eq. (1) [24,62]. The gravitational energy storage density ESD_g (kJ/kg) and volumetric energy storage density ESD_v (kWh/m^3) of the solid bed can be expressed by Eqs. (2) and (3), respectively.

$$Q_{dis} = \sum_{0}^{j=N} C_p\, q_m\, (T(t_i) - T_a)\Delta t \tag{1}$$

$$ESD_g = \frac{Q_{dis}}{m} \tag{2}$$

$$ESD_v = \frac{\rho_b\, ESD_g}{3600} \tag{3}$$

Where Q_{dis} is the useful sorption heat during discharge process (kJ), C_p is the specific heat capacity of the airflow (kJ/kg·K); q_m is the mass flow rate of the airflow (kg/s); $T(t_i)$ is the temperature of the fluidised bed (K) measured at the time of t_i; T_a is the inlet air temperature (K); Δt is the time interval between two consecutive temperature measurements (s); N is the number of time intervals; m is the sample's weight (kg); ρ_b the sample's bulk density (kg/m^3).

The mixing ratio (r), which is defined as the ratio of the mass of water vapour to the mass of dry air, can be calculated using Eqs. (4)–(6) [63–65]. The mixing ratios of the airflow at the inlet and outlet of the reactor are denoted as r_i and r_o. The ratio of the moisture concentration in the outlet air to that in the inlet air (CR) can be expressed by Eq. (7) [24]. When the CR reaches 1, the sample is considered completely hydrated.

$$r = \frac{\varepsilon\, e(T)}{p - e(T)} \tag{4}$$

$$\frac{RH}{100\%} = \frac{e(T)}{e_s(T)} \tag{5}$$

$$e_s(T) = c\, exp\left(\frac{a\,T}{T+b}\right) \tag{6}$$

$$CR = \frac{r_0}{r_i} \tag{7}$$

Where r is the mixing ratio of the moist air (kg/kg), $e(T)$ is the partial vapour pressure at a specific temperature (hPa), $e_s(T)$ is the saturation vapour pressure at a specific temperature (hPa), T is the temperature of the moist air (°C), p is the total air pressure (hPa), ε (0.622) is the ratio between the gas constants for dry air (287 J/kg K) and water vapour (461 J/kg K), a is 17.67, b is 243.5 (°C), c is 6.112 (hPa). Some studies suggested different constants to approximate $e_s(T)$, for example, a = 17.625, b = 243.04, c = 6.1094 for the temperature range of −40 and 50 °C [66].

3. Results and discussion

3.1. Material characteristics

The physical-chemical properties and water adsorption/desorption performance of the CMS-based salt composites at the material level have been characterized by our previous work [49]. Some of the experimental results are presented in Table 3. The CMS powder has an average pore size of 27.4 nm with a total pore volume of 1.79 cm^3/g. The large pore size and pore volume enable good dispersion and accessibility of the salt

Table 3
Characteristics of the CMS powder and the CMS-based salt composites.

Salt	S_{BET} (m^2/g)	V_{total} (cm^3/g)	Pore size (nm)	Experimental condition	Adsorption capacity (g/g)
CMS	283	1.79	27.4	30 °C	0.05
50 wt% $CaCl_2$/CMS	78	0.40	21.8	25 mbar H_2O	1.09
50 wt% $MgBr_2$/CMS	122	0.59	18.8		0.37
50 wt% $MgSO_4$/CMS	88	0.46	23.4		0.47

molecules on the pore walls of CMS, which were confirmed through scanning electron microscopy (SEM) and transmission electron microscopy (TEM) on the salt composites with salt loading levels of up to 50 wt% (or salt-to-CMS mass ratio of 1:1). Tested under the hydration conditions of 30 °C and 25 mbar partial vapour pressure, the $CaCl_2$/CMS composite with a salt loading level of 50 wt% provides the highest water adsorption capacity of 1.09 g/g, followed by the $MgSO_4$/CMS composite (0.47 g/g) and the $MgBr_2$/CMS composite (0.37 g/g). In terms of hydration kinetics, the $MgBr_2$/CMS composite shows the fastest water adsorption rate. Additionally, the large pore size and pore volume can benefit the dehydration process. For example, the salt/CMS composites are capable to desorb 70–80% of moisture at temperatures below 90 °C, while higher temperatures are required for the pure salts to achieve the similar dehydration levels. This indicates that the salt/CMS composites can be dehydrated using low-temperature heat sources. Besides, the salt/CMS composites display good reversibility over multiple adsorption-desorption cycles. The above results demonstrate that from a material characteristic perspective, the salt/CMS composites are potentially suitable for low temperature TCES. Nevertheless, their performance at the system level is unknown, including fluidisation behaviour, water sorption capacity and rate, ESD, temperature lift, and cyclic stability, which can be crucial information for the development of future fluidised-bed TCES systems. This information will be uncovered in the following sections.

3.2. Fluidisation behaviour

Prior to thermal characterization, the fluidisation behaviours of the sorption materials potentially suitable for FB-TCES, including CMS, zeolite 13X and their salt composites, were evaluated. The photos in Fig. 3 illustrate their fluidisation behaviours at different flow rates. For

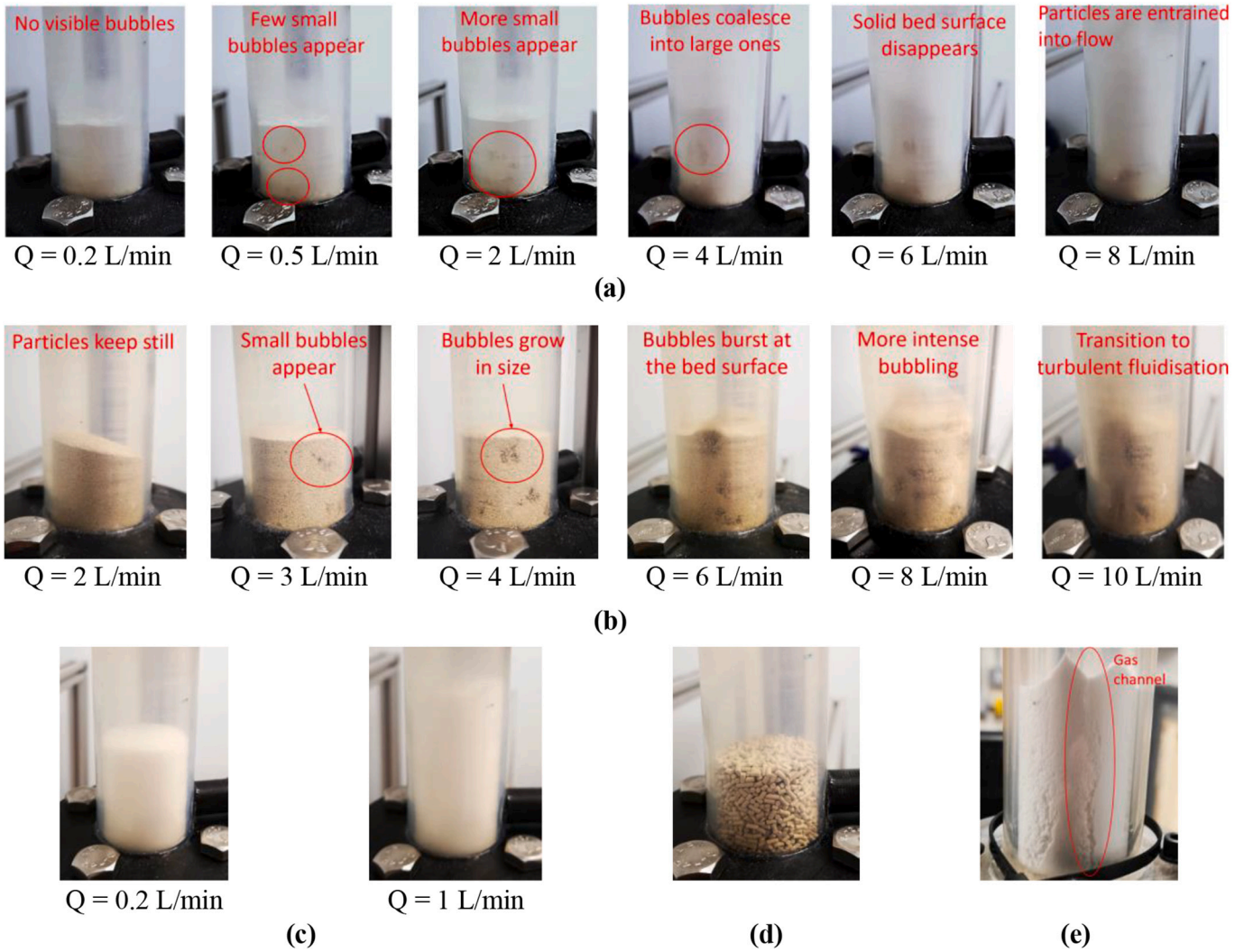

Fig. 3. Pictures showing the fluidisation characteristics of the (a) $CaCl_2$/CMS composite powder, (b) $CaCl_2$/zeolite composite powder, (c) pure CMS powder, (d) zeolite 13X pellets, and (e) $MgSO_4$ salt powder. (N.B., the pictures of zeolite 13X powder are not shown here, as it behaves almost identically to the $CaCl_2$/zeolite composite.)

the $CaCl_2$/CMS composite (with a salt loading level of 50 wt% and a particle size range of 150–300 μm), the solid bed remains stationary when the reactor is fed with dry air at flow rates below 0.5 L/min, as shown in Fig. 3a. Further increasing the flow rate induces bubbles to grow, coalesce along the reactor height and eventually burst at the bed surface. This process drives the solid motion, promoting the particles to recirculate in the bed. With the flow rate increased to 6 L/min, the bed surface vanishes, and the bed becomes more intensively fluidised. At the flow rate of 8 L/min, some particles begin to move with the gas stream and are carried away from the bed, a phenomenon known as the entrainment effect. Similar fluidisation behaviours were observed for the $MgSO_4$/CMS composite and the $MgBr_2$/CMS composite with a salt loading level of 50 wt%, which have similar particle sizes and particle densities as the $CaCl_2$/CMS composite.

In contrast, the CMS powder without salt impregnation begins to fluidise at a flow rate of 0.2 L/min. Moreover, the bed height increases significantly as the flow rate increases, as shown in Fig. 3c. The difference in bed height suggests that the CMS powder, being a type of Geldart Group A particles, undergoes smooth fluidisation with bed expansion before bubbling, while the salt/CMS composites belonging to Geldart Group B have small bubbles forming as soon as fluidisation begins [43,67]. Compared to the CMS powder, the salt/CMS composite require a higher flow rate (0.5 L/min) to initiate fluidisation, because of the increased particle density after salt impregnation, which necessitates a larger upward drag force to compensate the gravity force on the particles. On the other hand, the CMS powder is more easily entrained into high-speed airflow than the salt/CMS composites. For example, when tested at a flow rate of 6 L/min, a small portion of the CMS powder (about 7% of the total sample weight) escapes from the 300-mm-high reactor, while the particle loss of the $CaCl_2$/CMS composite is negligible.

As a reference sorption material, the $CaCl_2$/zeolite composite (with a particle size range of 212–425 μm and a salt loading level of 15 wt%) exhibits a similar fluidisation behaviour to that of the $CaCl_2$/CMS composite. However, the $CaCl_2$/zeolite composite requires a minimum flow rate of 3 L/min to reach the bubbling fluidisation state, as can be seen from Fig. 3b. The higher flow rate might be attributed to the higher particle density, because zeolite 13X is used as the porous matrix, which has a higher particle density than the CMS powder. We have also tested zeolite 13X pellets with a mean particle size of 1.6 mm (classified as Geldart group D particles) and pure salt such as $MgSO_4$ with particle sizes below 10 μm (classified as Geldart Group C particles) purchased from Sigma-Aldrich. Both materials are difficult to fluidise even at flow rates above 10 L/min, as shown in Fig. 3d and Fig. 3e. The above results demonstrate the crucial role of particle size and density in achieving effective fluidisation.

Fig. 4(a) shows the pressure drops across the solid beds of different sorption materials at flow rates ranging from 0 to 10 L/min, which were calculated using the measured data in Fig. S1. For all the materials (except the zeolite pellet), the pressure drop increases linearly with the flow rate initially, and then levels off, even with a further increase in flow rate after reaching the fluidisation state. The transition point corresponds to the minimum fluidisation condition. For example, the minimum fluidisation flow rate and velocity (u_{mf}) of the pure CMS powder at a sample weight of 30 g are approximately 0.2 L/min and 0.003 m/s, respectively. Beyond this point, the pressure drop stabilises at 240 Pa. When decreasing the sample weight to 15 g, the pressure drop of the CMS bed is halved while the minimum fluidisation flow rate remains the same. When replacing the CMS powder with a 30 g sample of the $CaCl_2$/CMS composite, there are slight increases in the minimum fluidisation flow rate to around 0.5 L/min (or the u_{mf} to 0.0075 m/s) and the pressure drop to 250 Pa. This indicates that the addition of 50 wt% $CaCl_2$ salt to the CMS powder has a minimal effect on the u_{mf} and pressure drop. In comparison, the minimum fluidisation flow rate of the $CaCl_2$/zeolite composite is approximately 3 L/min (equivalent to 0.045 m/s), six times that of the $CaCl_2$/CMS composite. The above findings support the image results in Fig. 3. It is worth noting that the solid beds experience more intense pressure fluctuations at flow rates exceeding 6 L/min. This may be resulted from the growth and eruption of large bubbles or the transition to the turbulent fluidisation regime [43]. In the following heat discharging tests, the flow rate of 6 L/min was chosen in order to achieve vigorous bubbling and sufficient gas-solid contact during hydration process.

Fig. 4(b) shows the dimensionless pressure drop ($\Delta P/\Delta P_0$) as a function of flow rate, where ΔP is the actual pressure drop across the bed and ΔP_0 is the pressure drop equal to the static weight of particles per unit area of the bed [54]. When $\Delta P/\Delta P_0 = 1$, the whole bed is fluidised [54]. It is clear that the bed of the pure CMS powder requires the lowest superficial gas velocity to be fully fluidised, followed by the $CaCl_2$/CMS composite powder, and then the zeolite 13X powder, while the zeolite 13X pellet cannot be fluidised at the given velocities.

3.3. Thermal energy storage performance

3.3.1. Salt/CMS composite materials

The salt composites consisting of $CaCl_2$, $MgSO_4$, and $MgBr_2$ with a salt loading level of 50 wt% were tested at 30 °C and 60% RH. The test

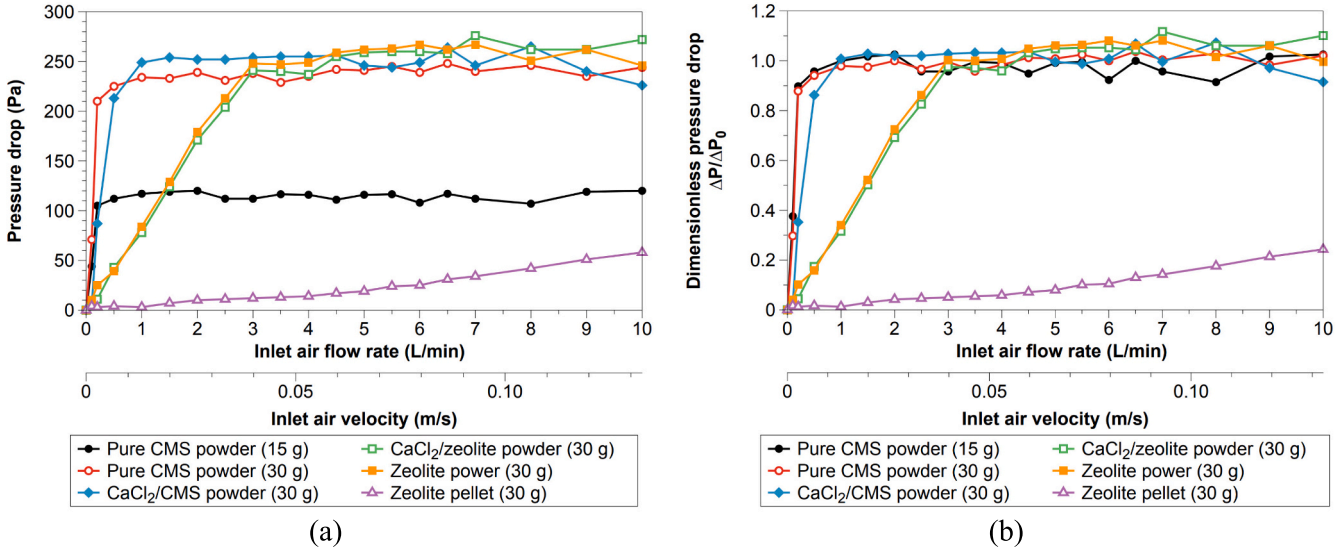

Fig. 4. (a) Actual pressure drops and (b) dimensionless pressure drops across the solid beds of the test materials as a function of flow rate.

conditions are consistent with the TGA tests conducted in our previous study. Fig. 5a shows the changes in bed temperature and outlet air humidity when the $CaCl_2$/CMS composite is being hydrated. The fluidised bed quickly heats up from around 29.2 to 57.5 °C when it comes into contact with moisture within the first 30 mins. The bed temperature then stabilises at 45.0 °C for about 4 h before gradually decreasing to the inlet air temperature. This suggests that the water sorption by the $CaCl_2$/CMS composite occurs in multiple stages: (1) the process starts with chemisorption, which quickly adsorbs all the moisture in the humid air; (2) then salt deliquescence and dissolution take place, which slow down the water adsorption process; (3) finally, the sorption process transitions to absorption, and the saturated salt solution becomes a diluted salt solution. The reduction in water sorption rate might be because water absorption is a bulk phenomenon and generally slower than surface adsorption. The water adsorption capacity of the $CaCl_2$/CMS composites estimated from the reactor test (i.e., the difference in moisture content between the inlet and outlet air) is approximately 0.92 g/g (see Fig. 6b and Table 4), which is slightly lower than the TGA result of 1.09 g/g.

With the chosen experimental conditions and sample weight in the fluidised bed system, the $CaCl_2$/CMS composite can achieve a maximum temperature lift of 28.1 °C. Along with the temperature measurement by using PT100 sensors, a thermal imaging camera was used to examine the temperature distribution of the solid bed under fluidisation and hydration. The uniform bed temperature distribution, as shown in Fig. 5b for example, indicates efficient heat and mass transfer within the fluidised bed.

The thermal performance of a salt composite is usually determined by the water sorption capacity and kinetics of its impregnated salt. In Table 3, it is evident that the salt/CMS composites prepared using $MgSO_4$ and $MgBr_2$ have significantly lower water adsorption capacities, compared to that using $CaCl_2$. Reflected in Fig. 6a are the lower maximum bed temperatures provided by the $MgSO_4$/CMS and $MgBr_2$/CMS composites, in comparison to the $CaCl_2$/CMS composite. The $MgBr_2$/CMS composite maintains the bed temperature above 39 °C for 1.5 h, while the $MgSO_4$/CMS composite provides a higher maximum bed temperature but a shorter useful heating time (i.e., only 15 mins with the temperatures above 39 °C). Being different from the multi-stage water sorption process observed for the $CaCl_2$/CMS composite, both the $MgSO_4$ and $MgBr_2$ based composites exhibit a single-stage water sorption process. For the $MgSO_4$/CMS composite, it exhibits a sharp temperature change similar to that of the $CaCl_2$/CMS composite at the beginning of hydration, indicating the occurrence of chemisorption without salt deliquescence. This is reasonable as the deliquescence relative humidity (DRH) of $MgSO_4$ is approximately 90% at 30 °C [68]. For the $MgBr_2$/CMS composite, it has a similar temperature variation trend to that of the $CaCl_2$/CMS composite in the middle and late stages, due to the fast kinetics and easy deliquescence of $MgBr_2$.

Among the three composite materials, the $MgSO_4$/CMS composite has the lowest total water uptake at 0.232 g/g, which is significantly lower than the TGA result of 0.47 g/g. That is presumably due to the slow kinetics of $MgSO_4$, which requires a longer time to reach its equilibrium adsorption capacity [49] (i.e., the CR has not reached 1 at the end of the test, see Fig. S2). In situations involving a large amount of $MgSO_4$ salt, such as in lab-scale reactor tests, the problem is more noticeable compared to TGA tests using milligram-weight samples.

Because of the largest water uptake, the $CaCl_2$/CMS composite takes the lead with a remarkable ESD of 1508 kJ/kg, exceeding that of the $MgBr_2$/CMS composite by three times and that of the $MgSO_4$/CMS composite by four times (see Table 4). It also outperforms many salt composites in the literature shown in Table 1. It is worth noting that the ESD was calculated using the air temperature measured above the fluidised bed. From Table 4 and Fig. S3, it is found that the air temperature is lower than the bed temperature, which is presumably due to the heat loss of the reactor. This heat loss could be reduced by carefully designing and optimising the fluidised bed reactor, so the actual ESDs of the proposed salt/CMS composites should be even higher than the values provided in this work.

In addition to ESD, cyclic stability is another key parameter to be considered in practical applications. As shown in Fig. 7a, the ESD of the $CaCl_2$/CMS composite remains similar after five consecutive cycles of heat charging and discharging. Moreover, there is no significant change in the fluidisation behaviour after 5 cycles, as depicted in Fig. 7b, suggesting the good stability of the $CaCl_2$/CMS composite for multi-cycle heat storage operation. Overall, the $CaCl_2$/CMS composite shows great potential for FB-TCES, and will be selected as a representative material to explore the potential of the salt/CMS composites when used in a FB-TCES system with different operating conditions.

3.3.2. *Effects of system operating conditions*

For real applications, it is not always possible to maintain the same operating conditions for the salt/CMS composites. For instance, the dehydration temperature from solar collectors might drop below 150 °C during cloudy days, and the hydration temperature of 30 °C might be unattainable in winter days without preheating the supplied air. Hence, further examination of the material was conducted with alternative operating conditions. Fig. 8a shows that the maximum bed temperature

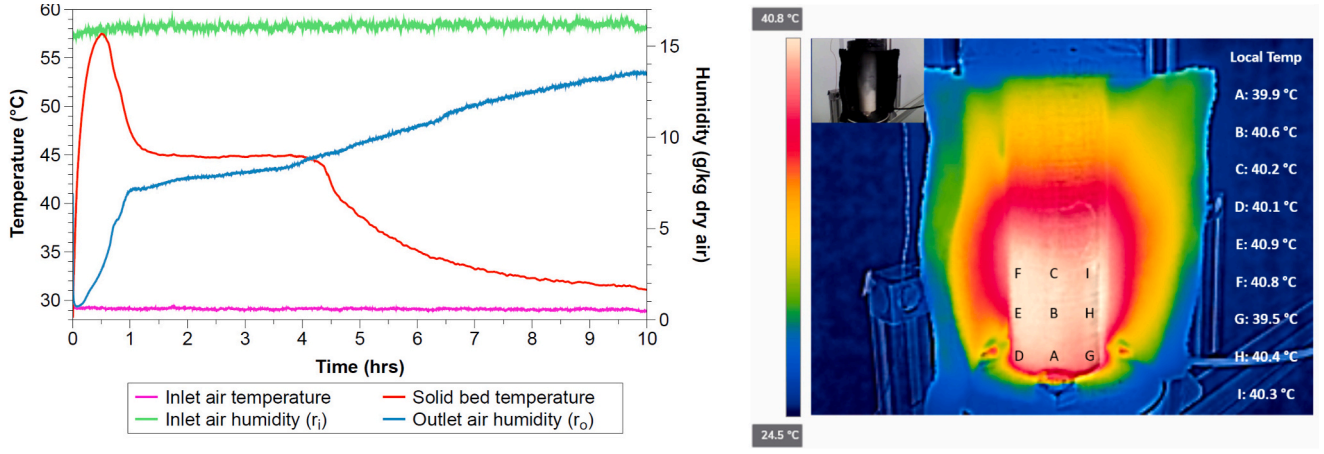

Fig. 5. (a) Bed temperature and humidity measurements for the $CaCl_2$/CMS composite powder, and (b) thermal image showing the temperature distribution of the fluidised bed reactor under the hydration conditions of 60% RH, 30 °C and 6 L/min.

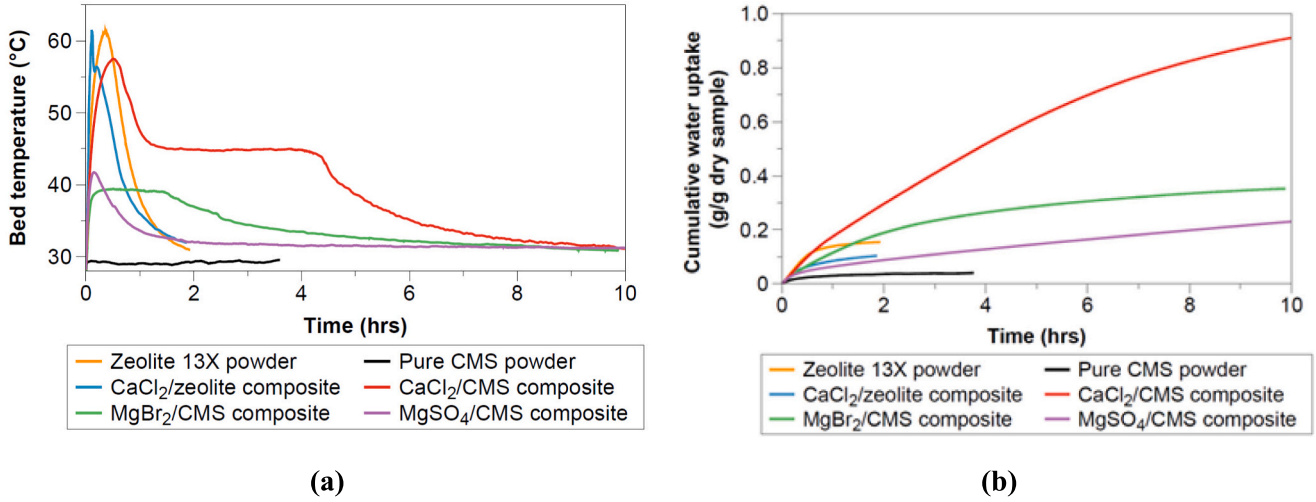

Fig. 6. Comparison between the sorption materials in terms of (a) bed temperature and (b) cumulative water uptake, when hydrated at 60% RH, 30 °C and 6 L/min.

Table 4
Summary of the performance of different sorption materials used in the FB-TCES system.

	$CaCl_2$/CMS	$MgBr_2$/CMS	$MgSO_4$/CMS
Bulk density (kg/m^3)	630	746	432
$\Delta T_{bed,\ max}$ (°C)	28.1	9.4	11.7
$\Delta T_{air,\ max}$ (°C)	20.9	7.2	9.1
Water uptake (g/g)	0.92	0.35	0.23
ESD_g (kJ/kg)	1508	474	368
ESD_v (kWh/m^3)	264	98	44

drops to 47.6 °C at the RH of 40% (or partial vapour pressure of 17.0 mbar), and further to 38.7 °C at the RH of 20% (or 8.5 mbar). This demonstrates the important role of partial vapour pressure in heat discharging performance. Along with RH, temperature is a factor in determining partial vapour pressure. Fig. 8b suggests that at the same RH of 60%, the temperature elevation decreases from 28.1 to 15.6 °C as the hydration temperature reduces from 30 to 18 °C (or equivalently the partial vapour pressure from 25.5 to 12.4 mbar). The impact of RH and hydration temperature on ESD is shown in Fig. 8e. In Section 3.2, it was found that the minimum flow rate required to fluidise the $CaCl_2$/CMS composite is 0.5 L/min. The fluidised bed shows vigorous bubbling for flow rates between 0.5 and 6 L/min, while noticeable pressure fluctuations and particle entrainment occur at higher flow rates. From a thermal perspective, increasing the flow rate from 2 to 6 L/min raises the maximum bed temperature from 46.0 to 57.5 °C, as can be seen from Fig. 8c. Using a flow rate of 10 L/min speeds up the completion of hydration (i.e., no temperature lift after 8 h), whereas it has a minimal effect on the maximum bed temperature. At the flow rate of 10 L/min, the material is fully hydrated and delivers an ESD of 1891 kJ/kg (see Fig. 8e). When considering both the fluidisation quality and thermal performance, it is recommended to use 6 L/min. It is worth noting that in different tests, the optimal flow rate may vary depending on the reactor size, sample weight and other factors.

The heat discharging performance is also influenced by the selection of dehydration temperature. It is evident from Fig. 8d and Fig. 8e that the ESD only decreases by 5.0% when using 120 °C instead of 150 °C for dehydration, even though the maximum bed temperature decreases by 6.4 °C. The peak shape in the temperature curve disappears when using a dehydration temperature of 100 °C, and the corresponding ESD is 19.7% lower than that at 150 °C. The ESD is reduced by 32.9% to around 1000 kJ/kg as the charging temperature is decreased to 80 °C. Although the $CaCl_2$/CMS composite could not be fully dehydrated at temperatures between 80 and 100 °C, it still maintains high ESDs with appreciable temperature lifts (10-15 °C). This stored energy might be contributed by the desorption of water molecules from the deliquescence or absorption process that have relatively weak chemical bonds with $CaCl_2$. The temperature lift of the $CaCl_2$/CMS composite at low charging temperatures could potentially be improved by carefully designing the fluidised

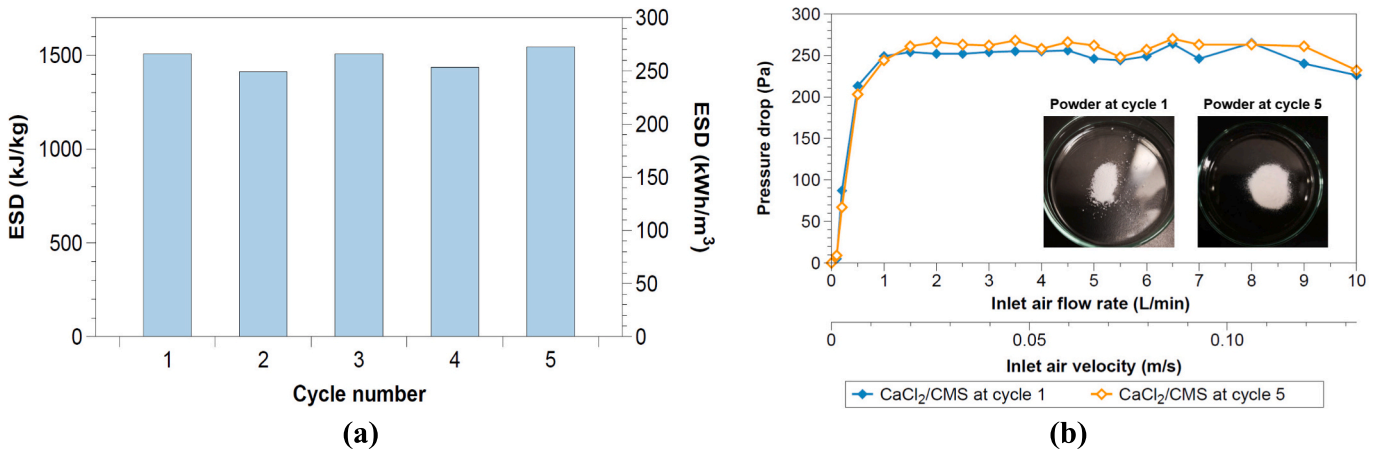

Fig. 7. (a) ESDs of the $CaCl_2$/CMS composite over 5 consecutive heat charging-discharging cycles; (b) pressure drops at different flow rates for the dehydrated $CaCl_2$/CMS composite sample at cycle 1 and cycle 5.

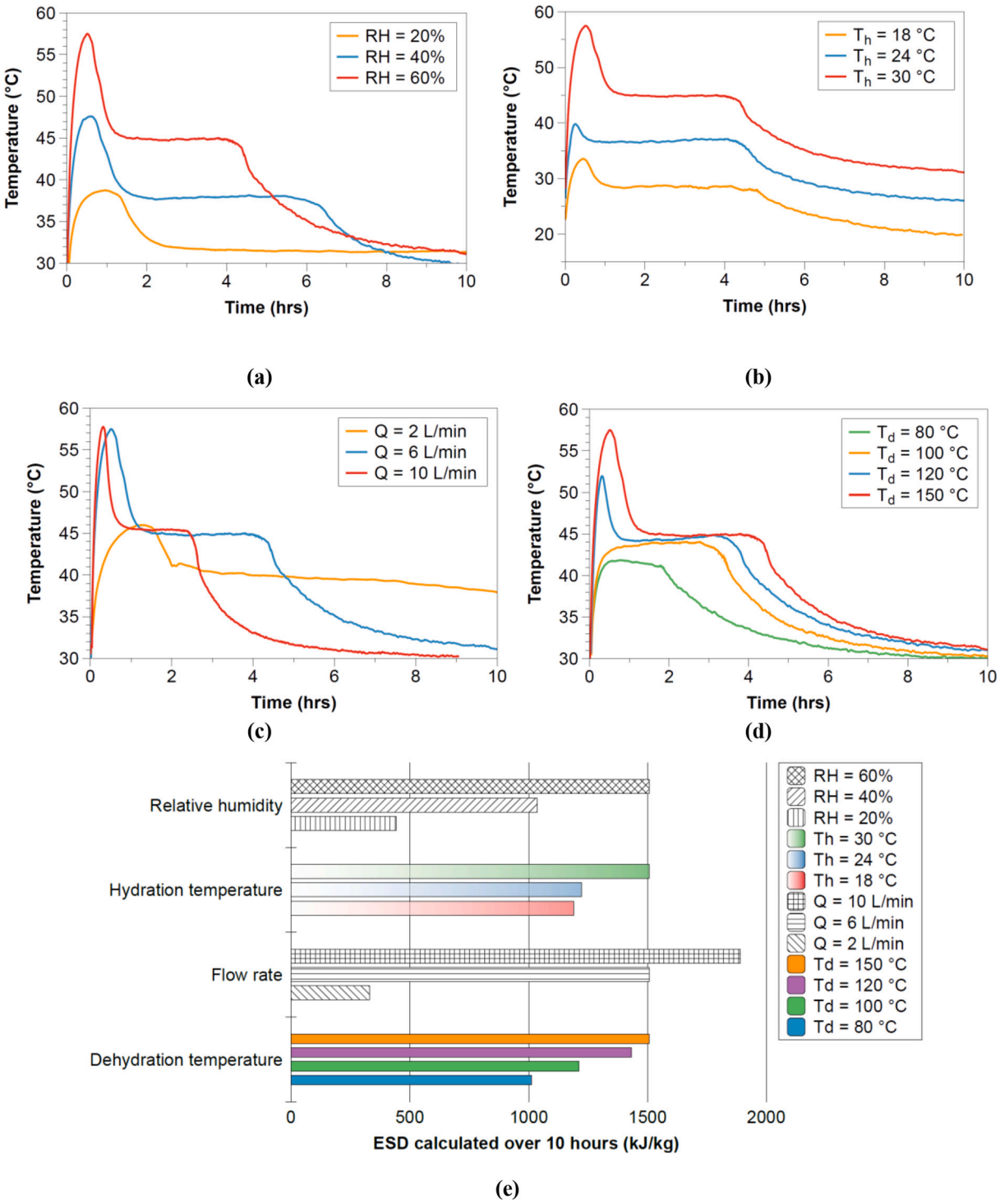

Fig. 8. Effects of different (a) RHs, (b) hydration temperatures, (c) flow rates, (d) dehydration temperatures on the thermal performance of the $CaCl_2$/CMS composite, and (e) its ESDs under different operating conditions. N.B., the baseline conditions are 60% (RH), 30 °C (hydration temperature), 6 L/min (flow rate) and 150 °C (dehydration temperature).

bed system and selecting appropriate hydration conditions. The above results confirm that the $CaCl_2$/CMS composite have great potential as a candidate material to store and recover low-grade heat.

3.3.3. *Comparison with other thermal energy storage materials*

In addition to the proposed salt/CMS composite, zeolite 13X is a porous sorption material that can be directly used in fluidised bed systems for low-temperature TCES. In this study, zeolite 13X powder (crushed from zeolite 13X pellets) and salt/zeolite composite powder derived from it were evaluated using the self-designed fluidised bed system. The result was compared to the salt/CMS composite results, to gain a better understanding of FB-TCES systems and their potential for future practical applications.

The thermal and water adsorption performance of the zeolite-based materials are shown in Figs. S5–7. When hydrated at the RH of 60%, the zeolite 13X powder can quickly raise the bed temperature to above 60 °C

in 20 mins, and the total water uptake is 0.155 g/g. Impregnating 15 wt % $CaCl_2$ into the zeolite 13X powder does not improve the performance. Instead, it leads to reductions in released air temperature, water uptake and ESD, but also makes moisture to penetrate the solid bed more easily (i.e., leading to an earlier breakthrough). The performance of the zeolite-based materials and the salt/CMS composites are compared in Fig. 6 and Figs. S2–3. For example, the $CaCl_2$/CMS composite provides a significantly higher water sorption capacity (0.922 g/g) and a similar maximum bed temperature (approximately 58 °C), compared to the zeolite 13X powder (0.155 g/g and 61.3 °C). At the same sample mass of 30 g, the heat discharging time of the zeolite 13X powder is approximately 2 h, whereas the $CaCl_2$/CMS composite can maintain heat release for 10 h. Correspondingly, the zeolite 13X powder has an ESD of 245 kJ/kg, while the ESD of the $CaCl_2$/CMS composite reaches up to 1508 kJ/kg under similar conditions.

In this research, the $CaCl_2$ based composites were hydrated at a moderate RH of 60%, in order to avoid severe deliquescence and prevent $CaCl_2$ from leaking out of the pores at high RHs. As a stable physical moisture sorbent, zeolite 13X does not have such problem. Therefore, a much higher RH can be used to hydrate the zeolite 13X powder. As shown in Fig. S5, the zeolite 13X powder quickly reaches a maximum bed temperature of 69.3 °C at the RH of 85%, which is higher than the values of the $CaCl_2$/CMS composite and the zeolite 13X powder tested at the RH of 60%. Since the zeolite-13X-based system can achieve both high discharging temperatures (>60 °C) and heating rates, it can work as a fast discharge-charge thermal battery for medium-temperature applications such as hot water production. However, the zeolite 13X powder needs high charging temperatures (at least 150 °C) for efficient heat storage [25]. In comparison, the salt/CMS composites offer relatively lower heating rates and discharging temperatures (40–60 °C), but have much higher ESDs and require lower regeneration temperatures. Therefore they are more suitable for low-temperature and large-scale TCES applications such as integrating with solar air heating systems or heat recovery systems for space heating.

Although fluidised-bed thermal energy storage (FB-TES) systems offer numerous benefits, there have been few TES materials available that can meet the fluidisation and energy storage criteria. Granular phase change material (PCM) is one of the most widely researched materials for low-temperature FB-TES systems. However, most of the granular PCMs reported, including the commercial products 'GR bound PCMs', still encounter issues such as particle agglomeration and gas channel formation in fluidised beds (caused by particle abrasion and paraffin liquid leakage), and have low ESDs (e.g., 44 kJ/kg for GR 50) [69,70]. For the first time, this work successfully demonstrates thermal energy storage using a fluidised bed system with a high-performance composite made of a commercial mesoporous silica and salt hydrate. Among the proposed materials, the $CaCl_2$/CMS composite stands out for its exceptional ESD of up to 1900 kJ/kg, high heat discharging temperatures of up to 58 °C, and better thermal-physical stability compared to the traditional granular PCMs. What is more, the material can be charged at temperatures of 80–100 °C, while still achieving ESDs of over 1000 kJ/kg, more than half of its maximum ESD. At these medium charging temperatures, the $CaCl_2$/CMS composite can provide temperature lifts of 11–15 °C during hydration, which can be used for space heating or for pre-charging the salt/CMS composites before exposing the materials to a heat source with a temperature of 150 °C or above. This finding suggests that the $CaCl_2$/CMS composite has great potential for recovering low-grade heat (<100 °C) and also for directly harvesting solar energy. Furthermore, the simple fabrication procedure and the use of readily available, cost-effective porous matrix and salt hydrates allow for mass production of the composite materials and scalability of FB-TES systems. A conceptual design of a $CaCl_2$/CMS composite integrated FB-TES system for domestic heating is shown in Fig. S8.

4. Conclusions

This study presents a new approach to store thermal energy by using a fluidised bed thermochemical energy storage (FB-TCES) system with a "salt in porous matrix" composite. Among various porous materials, a commercial mesoporous silica (CMS) powder with an average pore size of 27.4 nm and particle sizes of 150–300 μm was selected as the host matrix for salt impregnation. Three composites based on CMS with different salts, specially $CaCl_2$, $MgSO_4$ and $MgBr_2$, with the same salt content of 50 wt%, were prepared using an incipient wetness impregnation technique. A laboratory prototype FB-TCES system was constructed to evaluate the materials in terms of fluidisation behaviour, thermal performance, water adsorption capacity and kinetics, and energy storage density (ESD). The main conclusions are as follows:

- The salt/CMS composite particles belong to Geldart Group B with a minimum fluidisation velocity (u_{mf}) of around 0.01 m/s. Once the superficial gas velocity exceeds u_{mf}, the particle bed transitions to the bubbling fluidisation regime. The vigorous bubbling and solid mixing promote an even distribution of bed temperature during the exothermic hydration process.
- When hydrated at 30 °C with a partial vapour pressure of 25 mbar, the $CaCl_2$/CMS composite provides a maximum bed temperature of 57.5 °C, a total water uptake of 0.92 g/g and an ESD of 1508 kJ/kg. The ESD value exceeds that of the $MgBr_2$/CMS composite by three times and that of the $MgSO_4$/CMS composite by four times.
- The $CaCl_2$/CMS composite can be regenerated using low-temperature heat sources (below 100 °C) while still achieving high ESDs (over 1000 kJ/kg). Adjusting the system operating conditions such as hydration temperature or humidity is an effective measure to control the temperature lift and thermal power output.
- The zeolite 13X powder is suitable for FB-TCES applications that require fast heat discharging and high temperature lifts. In contrast, the salt/CMS composite powders, which have lower dehydration temperatures, higher ESDs and lower costs, are more suitable for low-grade heat harvesting and large-scale applications.

Overall, using the $CaCl_2$/CMS composite based fluidised bed system shows promise as a solution for storing thermal energy at low temperatures. The above conclusions were drawn from the tests using a small sample weight (30 g), a small-scale reactor (300 mm height and 40 mm diameter), a limited number of test materials, and a vacuum oven for dehydration. For a more comprehensive feasibility analysis, it is recommended to scale up the fluidised bed system and integrate it with the building facilities such as solar thermal collectors or electric heaters to charge the materials. A wider variety of CSPMs, made from different salt hydrates and porous matrices with varying salt loading levels, should be tested and compared. The fluidised bed system needs to be designed and operated carefully (in terms of material weight, reactor shape and dimensions, de/hydration time, etc.) to ensure stable and high thermal output, prevent excessive heat loss, and minimise the occurrence of overhydration, salt solution leakage, particle aggregation, and corrosion. Further investigations include evaluating the technical and economic viability of using this technology in buildings. These will require conducting building energy simulation, on-site measurement, and life cycle cost assessment.

CRediT authorship contribution statement

Xiao Liu: Writing – review & editing, Writing – original draft, Methodology, Investigation, Conceptualization. **Xin Liu:** Writing – review & editing, Writing – original draft, Methodology, Investigation, Conceptualization. **Fangming Yang:** Writing – review & editing, Writing – original draft, Methodology, Investigation. **Yupeng Wu:** Writing – review & editing, Supervision, Resources, Funding acquisition, Conceptualization.

Declaration of competing interest

The authors declare that they have no known competing financial interests or personal relationships that could have appeared to influence the work reported in this paper.

Data availability

Data will be made available on request.

Acknowledgment

This work was supported by the Engineering and Physical Sciences Research Council, UK [grant number EP/S030786/1]. This work was supported by the Centre for Postdoctoral Development in Infrastructure, Cities and Energy (C-DICE). C-DICE is funded by the Research England Development Fund.

Appendix A. Supplementary data

Supplementary data to this article can be found online at https://doi.org/10.1016/j.apenergy.2024.122953.

References

[1] Charlesworth G. Decarbonising heat in Britain's buildings. Building Research Establishment (BRE) Group; 2022.
[2] Köll R, van Helden W, Engel G, Wagner W, Dang B, Jänchen J, et al. An experimental investigation of a realistic-scale seasonal solar adsorption storage system for buildings. Solar Energy 2017;155:388–97.
[3] Zhang Y, Chen Z, Kutlu C, Su Y, Riffat S. Investigation on a vermiculite-based solar thermochemical heat storage system for building applications. Future Cities Environ 2022;8(1):8.
[4] Li T, Wu M, Xu J, Du R, Yan T, Wang P, et al. Simultaneous atmospheric water production and 24-hour power generation enabled by moisture-induced energy harvesting. Nat Commun 2022;13(1):6771.
[5] Li TX, Xu JX, Yan T, Wang RZ. Development of sorption thermal battery for low-grade waste heat recovery and combined cold and heat energy storage. Energy 2016;107:347–59.
[6] Chao J, Xu J, Xiang S, Bai Z, Yan T, Wang P, et al. High energy-density and power-density cold storage enabled by sorption thermal battery based on liquid-gas phase change process. Appl Energy 2023;334:120656.
[7] Ferrucci F, Stitou D, Ortega P, Lucas F. Mechanical compressor-driven thermochemical storage for cooling applications in tropical insular regions. Concept and efficiency analysis. Appl Energy 2018;219:240–55.
[8] Li W, Luo X, Yang P, Wang Q, Zeng M, Markides CN. Solar-thermal energy conversion prediction of building envelope using thermochemical sorbent based on established reaction kinetics. Energ Conver Manage 2022;252:115117.
[9] Li W, Klemeš JJ, Wang Q, Zeng M. Salt hydrate–based gas-solid thermochemical energy storage: current progress, challenges, and perspectives. Renew Sustain Energy Rev 2022;154:111846.
[10] N'Tsoukpoe KE, Liu H, Pierrès NL, Luo L. A review on long-term sorption solar energy storage. Renew Sustain Energy Rev 2009;13(9):2385–96.
[11] Scapino L, Zondag HA, Van Bael J, Diriken J, Rindt CCM. Sorption heat storage for long-term low-temperature applications: a review on the advancements at material and prototype scale. Appl Energy 2017;190:920–48.
[12] Clark R-J, Mehrabadi A, Farid M. State of the art on salt hydrate thermochemical energy storage systems for use in building applications. J Energy Storage 2020;27:101145.
[13] Zhang Y, Wang R. Sorption thermal energy storage: concept, process, applications and perspectives. Energy Storage Mater 2020;27:352–69.
[14] Wu H, Salles F, Zajac J. A critical review of solid materials for low-temperature thermochemical storage of solar energy based on solid-vapour adsorption in view of space heating uses. Molecules 2019;24(5):945.
[15] Kuznik F, Johannes K, Obrecht C, David D. A review on recent developments in physisorption thermal energy storage for building applications. Renew Sustain Energy Rev 2018;94:576–86.
[16] Whiting GT, Grondin D, Stosic D, Bennici S, Auroux A. Zeolite–MgCl2 composites as potential long-term heat storage materials: influence of zeolite properties on heats of water sorption. Solar Energy Mater Solar Cells 2014;128:289–95.
[17] Feng C, E J, Han W, Deng Y, Zhang B, Zhao X, et al. Key technology and application analysis of zeolite adsorption for energy storage and heat-mass transfer process: a review. Renew Sustain Energy Rev 2021;144:110954.
[18] Structure Commission of the International Zeolite Association (IZA-SC). Database of zeolite structures [cited 2023.11.19; Available from, http://www.iza-structure.org/databases/; 2017.
[19] Touloumet Q, Postole G, Massin L, Lorentz C, Auroux A. Investigation of the impact of zeolite shaping and salt deposition on the characteristics and performance of composite thermochemical heat storage systems. J Mater Chem A 2023;11(6):2737–53.
[20] Wang C, Leng S, Guo H, Yu J, Li W, Cao L, et al. Quantitative arrangement of Si/Al ratio of natural zeolite using acid treatment. Appl Surf Sci 2019;498:143874.
[21] Mette B, Kerskes H, Drück H, Müller-Steinhagen H. Experimental and numerical investigations on the water vapor adsorption isotherms and kinetics of binderless zeolite 13X. Int J Heat Mass Transf 2014;71:555–61.
[22] Padamurthy A, Nandanavanam J, Rajagopalan P. Sustainable and open sorption system for low-temperature heat storage applications. Int J Energy Res 2022;1:17.
[23] Mahon D, Claudio G, Eames PC. An experimental investigation to assess the potential of using MgSO4 impregnation and Mg2+ ion exchange to enhance the performance of 13X molecular sieves for interseasonal domestic thermochemical energy storage. Energ Conver Manage 2017;150:870–7.
[24] Bardy DA, Cruickshank CA, Tezel FH, Carrier YH, Wong B. An experimental investigation of fixed and fluidized beds as adsorbers in compact thermal energy storage systems. J Energy Storage 2020;31:101648.
[25] Kohler T, Müller K. Influence of different adsorbates on the efficiency of thermochemical energy storage. Energy Sci Eng 2017;5(1):21–9.
[26] Hongois S, Kuznik F, Stevens P, Roux J-J. Development and characterisation of a new MgSO4−zeolite composite for long-term thermal energy storage. Solar Energy Mater Solar Cells 2011;95(7):1831–7.
[27] van Essen VM, Zondag HA, Gores JC, Bleijendaal LPJ, Bakker M, Schuitema R, et al. Characterization of MgSO4 hydrate for thermochemical seasonal heat storage. J Solar Energy Eng 2009;131(4):041014.
[28] Xu SZ, Wang RZ, Wang LW, Zhu J. Performance characterizations and thermodynamic analysis of magnesium sulfate-impregnated zeolite 13X and activated alumina composite sorbents for thermal energy storage. Energy 2019;167:889–901.
[29] Bertsch F, Mette B, Asenbeck S, Kerskes H, Müller-Steinhagen H. Low temperature chemical heat storage - an investigation of hydration reactions. 2009.
[30] Heijmans K, Nab S, Holkenborg BK, Pathak AD, Gaastra-Nedea S, Smeulders D. Development of a reactive force field for CaCl2· nH2O, and the application to thermochemical energy storage. Comput Mater Sci 2021;197:110595.
[31] Whiting G, Grondin D, Bennici S, Auroux A. Heats of water sorption studies on zeolite–MgSO4 composites as potential thermochemical heat storage materials. Solar Energy Mater Solar Cells 2013;112:112–9.
[32] Liu X, Wang H, Liu X, Yang F, Guan L, Sani S, et al. Development of MgSO4/mesoporous silica composites for thermochemical energy storage: the role of porous structure on water adsorption. Energy Rep 2022;8:4913–21.
[33] Nonnen T, Preißler H, Kött S, Beckert S, Gläser R. Salt inclusion and deliquescence in salt/zeolite X composites for thermochemical heat storage. Microporous Mesoporous Mater 2020;303:110239.
[34] Nonnen T, Beckert S, Gleichmann K, Brandt A, Unger B, Kerskes H, et al. A thermochemical long-term heat storage system based on a salt/zeolite composite. Chem Eng Technol 2016;39(12):2427–34.
[35] Zheng X, Ge TS, Wang RZ, Hu LM. Performance study of composite silica gels with different pore sizes and different impregnating hygroscopic salts. Chem Eng Sci 2014;120:1–9.
[36] Zhu J, Gao C, Kong F, Zhang K, Bai Z, Guo J. Low-priced stable SrCl2@SG composite sorbents for low-grade solar heat storage application in open sorption systems. Solar Energy Mater Solar Cells 2021;229:111118.
[37] Gaeini M, Rouws AL, Salari JWO, Zondag HA, Rindt CCM. Characterization of microencapsulated and impregnated porous host materials based on calcium chloride for thermochemical energy storage. Appl Energy 2018;212:1165–77.
[38] Courbon E, D'Ans P, Permyakova A, Skrylnyk O, Steunou N, Degrez M, et al. Further improvement of the synthesis of silica gel and CaCl2 composites: enhancement of energy storage density and stability over cycles for solar heat storage coupled with space heating applications. Solar Energy 2017;157:532–41.
[39] Shi W, Zhu Y, Shen C, Shi J, Xu G, Xiao X, et al. Water sorption properties of functionalized MIL-101(Cr)-X (X=-NH2, –SO3H, H, –CH3, –F) based composites as thermochemical heat storage materials. Microporous Mesoporous Mater 2019;285:129–36.
[40] Touloumet Q, Silvester L, Bois L, Postole G, Auroux A. Water sorption and heat storage in CaCl 2 impregnated Aluminium fumarate MOFs. Solar Energy Mater Solar Cells 2021;231:111332.
[41] Baeyens J, Shuo L, Dewil R, Zhang H, Deng Y. Fluidized bed technology: challenges and perspectives. IOP Conf Ser Earth Environ Sci 2022;952(1):012010.
[42] Almendros-Ibáñez JA, Fernández-Torrijos M, Díaz-Heras M, Belmonte JF, Sobrino C. A review of solar thermal energy storage in beds of particles: packed and fluidized beds. Solar Energy 2019;192:193–237.
[43] Marie LF, Landini S, Bae D, Francia V, O'Donovan TS. Advances in thermochemical energy storage and fluidised beds for domestic heat. J Energy Storage 2022;53:105242.
[44] Kant K, Pitchumani R. Advances and opportunities in thermochemical heat storage systems for buildings applications. Appl Energy 2022;321:119299.
[45] Solé A, Martorell I, Cabeza LF. State of the art on gas–solid thermochemical energy storage systems and reactors for building applications. Renew Sustain Energy Rev 2015;47:386–98.
[46] Pardo P, Anxionnaz-Minvielle Z, Rougé S, Cognet P, Cabassud M. Ca(OH)2/CaO reversible reaction in a fluidized bed reactor for thermochemical heat storage. Solar Energy 2014;107:605–16.
[47] Marie LF, O'Donovan TS. Fluidisation of thermochemical energy storage materials: degradation assessment. Energy Sour Part A Recover Util Environ Eff 2023;45(4):10034–50.
[48] Sabiha MA, Saidur R, Mekhilef S, Mahian O. Progress and latest developments of evacuated tube solar collectors. Renew Sustain Energy Rev 2015;51:1038–54.

[49] Wang H, Liu X, Liu X, Sun C, Wu Y. Fluidizable mesoporous silica composites for thermochemical energy storage. Energy 2023:127255.
[50] Li TX, Wu S, Yan T, Xu JX, Wang RZ. A novel solid–gas thermochemical multilevel sorption thermal battery for cascaded solar thermal energy storage. Appl Energy 2016;161:1–10.
[51] Zhou Y, Zhu J. A review on fluidization of Geldart Group C powders through nanoparticle modulation. Powder Technol 2021;381:698–720.
[52] Raganati F, Chirone R, Ammendola P. Gas–solid fluidization of cohesive powders. Chem Eng Res Des 2018;133:347–87.
[53] Zhu X, Zhang Q, Wang Y, Wei F. Review on the nanoparticle fluidization science and technology. Chin J Chem Eng 2016;24(1):9–22.
[54] Raganati F, Chirone R, Ammendola P. Calcium-looping for thermochemical energy storage in concentrating solar power applications: evaluation of the effect of acoustic perturbation on the fluidized bed carbonation. Chem Eng J 2020;392:123658.
[55] Raganati F, Ammendola P, Chirone R. Role of acoustic fields in promoting the gas-solid contact in a fluidized bed of fine particles. KONA Powd Part J 2015;32(0):23–40.
[56] Zhang YN, Wang RZ, Zhao YJ, Li TX, Riffat SB, Wajid NM. Development and thermochemical characterizations of vermiculite/SrBr2 composite sorbents for low-temperature heat storage. Energy 2016;115:120–8.
[57] Zhao YJ, Wang RZ, Zhang YN, Yu N. Development of SrBr2 composite sorbents for a sorption thermal energy storage system to store low-temperature heat. Energy 2016;115:129–39.
[58] D'Ans P, Courbon E, Permyakova A, Nouar F, Simonnet-Jégat C, Bourdreux F, et al. A new strontium bromide MOF composite with improved performance for solar energy storage application. J Energy Storage 2019;25:100881.
[59] Ji W, Zhang H, Liu S, Wang Z, Deng S. An experimental study on the binary hydrated salt composite zeolite for improving thermochemical energy storage performance. Renew Energy 2022;194:1163–73.
[60] Liu H, Nagano K, Sugiyama D, Togawa J, Nakamura M. Honeycomb filters made from mesoporous composite material for an open sorption thermal energy storage system to store low-temperature industrial waste heat. Int J Heat Mass Transf 2013;65:471–80.
[61] Gao N, Deng L, Li J, Huang H, Zhou B, Zhou Y. Multi-form heat storage performance of expanded graphite based CaCl2 composites for low-grade heat source. Energy Rep 2022;8:12117–25.
[62] Strong C, Carrier Y, Handan Tezel F. Experimental optimization of operating conditions for an open bulk-scale silica gel/water vapour adsorption energy storage system. Appl Energy 2022;312:118533.
[63] Bolton D. The computation of equivalent potential temperature. Mon Weather Rev 1980;108(7):1046–53.
[64] Lawrence MG. The relationship between relative humidity and the dewpoint temperature in moist air: a simple conversion and applications. Bull Am Meteorol Soc 2005;86(2):225–33.
[65] Nugent A, DeCou D, Russell S, Karamperidou C. Atmospheric processes and phenomena. Hawaii: Outreach College, University of Hawaii at Manoa; 2019.
[66] Alduchov OA, Eskridge RE. Improved Magnus form approximation of saturation vapor pressure. J Appl Meteorol 1996;35(4):601–9.
[67] Geldart D. Types of gas fluidization. Powder Technol 1973;7(5):285–92.
[68] Posern K, Kaps C. Humidity controlled calorimetric investigation of the hydration of MgSO4 hydrates. J Therm Anal Calorim 2008;92(3):905–9.
[69] Belmonte JF, Izquierdo-Barrientos MA, Molina AE, Almendros-Ibáñez JA. Air-based solar systems for building heating with PCM fluidized bed energy storage. Energ Buildings 2016;130:150–65.
[70] Izquierdo-Barrientos MA, Sobrino C, Almendros-Ibáñez JA, Barreneche C, Ellis N, Cabeza LF. Characterization of granular phase change materials for thermal energy storage applications in fluidized beds. Appl Energy 2016;181:310–21.